












Latitudinal patterns in ocean C:N:P reflect phytoplankton acclimation and macromolecular composition

Justin D. Liefer^{a,1} , Angelicque E. White^b , Zoe V. Finkel^c , Andrew J. Irwin^d , Mathilde Dugenne^b, Keisuke Inomura^e , François Ribalet^f , E. Virginia Armbrust^f , David M. Karl^b , Matthew H. Fyfe^g, Christopher M. Brown^g, and Michael J. Follows^h 

Affiliations are included on p. 8.

Edited by James Galloway, University of Virginia, Charlottesville, VA; received March 2, 2024; accepted October 1, 2024

The proportions of carbon (C), nitrogen (N), and phosphorus (P) in surface ocean particulate matter deviate greatly from the canonical Redfield Ratio (C:N:P = 106:16:1) in space and time with significant implications for global carbon storage as this matter reaches the deep ocean. Recent work has revealed clear latitudinal patterns in C:N:P, yet the relative importance of ecological, physiological, or biochemical processes in creating these patterns is unclear. We present high-resolution, concurrent measurements of particulate C:N:P, macromolecular composition, environmental conditions, and plankton community composition from a transect spanning a subtropical-subpolar boundary, the North Pacific Transition Zone. We find that the summed contribution of macromolecules to particulate C, N, and P is consistent with, and provides interpretation for, particulate C:N:P patterns. A decline in particulate C:N from the subtropical to subpolar North Pacific largely reflects an increase in the relative contribution of protein compared to carbohydrate and lipid, whereas variation in C:P and N:P correspond to shifts in protein relative to polyphosphate, DNA, and RNA. Possible causes for the corresponding trends in C:N and macromolecular composition include physiological responses and changes in community structure of phytoplankton, which represented approximately 1/3rd of particulate C across the transect. Comparison with culture experiments and an allocation-based model of phytoplankton macromolecular composition suggest that physiological acclimation to changing nutrient supply is the most likely explanation for the latitudinal trend in C:N, offering both a mechanistic interpretation and biochemical basis for large-scale patterns in C:N:P.

elemental stoichiometry | phytoplankton | nutrients | acclimation

The elemental stoichiometry (carbon:nitrogen:phosphorus; C:N:P) of particulate matter sinking from the surface ocean affects fundamental global processes including how efficiently atmospheric C can be sequestered in the deep ocean (1). Redfield (2) identified a mean C:N:P of marine particulate matter of 106:16:1 (the Redfield Ratio) that has often been treated as a constant in models of the global carbon cycle. Recent studies show that surface particulate C:N:P varies widely and systematically across the ocean as C:N, C:P, and N:P generally exceed Redfield proportions in subtropical regions and fall below these proportions in high-latitude and equatorial upwelling regions (3–5). Building on these observations, newer models that utilize a flexible particulate C:N:P suggest that materials exported from the surface ocean are more C-rich and result in greater carbon storage capacity for the ocean relative to a world with a fixed particulate C:N:P (6, 7). Yet observational coverage of surface ocean particulate stoichiometry is sparse and the drivers of its variability are not well understood. Due to this constraint, as well as computational costs, many climate and carbon cycle models still represent particulate matter with a fixed Redfield Ratio.

The C:N:P of surface particulate matter has been proposed to mainly reflect its macromolecular composition rather than its content of small monomeric organic matter or inorganic material. Wakeham et al. (8) showed that carbohydrates, amino acids, lipids, and pigments account for >80% of particulate organic carbon in the surface waters of the central equatorial Pacific. However, a complete macromolecular basis for surface particulate C:N:P has not been demonstrated since previous field studies (compiled in *SI Appendix, Table S1*) have not measured C, N, and P in parallel with all major macromolecules that contribute to these elements.

Phytoplankton are a major component of surface particulate matter and the ultimate source of organic material that is consumed and transformed by heterotrophs. The elemental composition of phytoplankton reflects their macromolecular allocation to C-rich carbohydrates and lipids, N-rich proteins, and P-rich nucleic acids and polyphosphate

Significance

The chemical composition of ocean particulate matter varies among ocean regions, with major implications for ocean carbon storage. However, this particulate matter is typically assigned a mean C:N:P (106:16:1, the Redfield Ratio) in models of the global carbon cycle since a mechanistic understanding of ocean C:N:P patterns is elusive yet also critical for developing predictive models. We show that the C:N:P of surface ocean particulate matter reflects changes in its content of major biomolecules like proteins, carbohydrates, and lipids along an environmental gradient. This C:N:P variation is also predictable based on how phytoplankton adjust their content of major biomolecules in response to environmental conditions, highlighting a possible mechanism for ocean C:N:P patterns that can be used in carbon cycle models.

Author contributions: J.D.L., A.E.W., Z.V.F., A.J.L., and M.J.F. designed research; J.D.L., A.E.W., M.D., F.R., E.V.A., D.M.K., M.H.F., and C.M.B. performed research; C.M.B. contributed new reagents/analytic tools; J.D.L., A.E.W., Z.V.F., A.J.L., M.D., and K.I. analyzed data; K.I. and M.J.F. contributed modeling; and J.D.L. wrote the paper.

The authors declare no competing interest.

This article is a PNAS Direct Submission.

Copyright © 2024 the Author(s). Published by PNAS. This article is distributed under [Creative Commons Attribution-NonCommercial-NoDerivatives License 4.0 \(CC BY-NC-ND\)](https://creativecommons.org/licenses/by-nc-nd/4.0/).

¹To whom correspondence may be addressed. Email: jlief@mta.ca.

This article contains supporting information online at <https://www.pnas.org/lookup/suppl/doi:10.1073/pnas.2404460121/-/DCSupplemental>.

Published November 5, 2024.

storage bodies (9). There are systematic differences in the C:N:P of major phytoplankton taxa (10, 11) that correspond to their underlying macromolecular composition (12), so biogeographical variations in phytoplankton community structure could contribute significantly to spatial trends in C:N:P (3, 5, 13, 14). Phytoplankton also reallocate their macromolecular content according to environmental conditions, changes in growth rate, and to form “luxury” stores of nonlimiting elements (15, 16) leading to large variations in elemental composition. Variations of threefold in phytoplankton C:N and more than 10-fold in C:P occur as a function of nutrient supply (17–19) with smaller variations as a function of light intensity or temperature (19, 20), suggesting that physiological acclimation may profoundly impact surface ocean particulate stoichiometry (21, 22). Zooplankton consumers and bacterial decomposers may also make an important contribution to bulk particulate matter and its C:N:P (23, 24), as would their differential remineralization of particulate substrates (25, 26). The detritus from phytoplankton and heterotrophic plankton also makes a large contribution to surface particulate matter and is estimated to comprise >50% of surface particulate organic carbon (27–29). Although the biochemical nature of this detritus is poorly understood, it may also affect large-scale C:N:P patterns (30, 31).

Through measurements made along an environmental gradient in the North Pacific Ocean we address two key hypotheses that emerge from the review above:

- Large-scale horizontal gradients in surface ocean particulate C:N:P can be explained by changes in the relative abundance of major macromolecules like protein, carbohydrate, lipid, DNA, RNA, and pigment.
- Variations in the macromolecular content of phytoplankton driven by physiological acclimation can explain and predict patterns in surface ocean C:N:P.

We measured the C:N:P and macromolecular composition of surface (~6 m depth) particulate matter, plankton community composition, and environmental variables along a meridional

transect (158°W) in the North Pacific Ocean from ~25 to 42°N. The transect spans the transition zone (TZ)-chlorophyll front and passes from the oligotrophic subtropical gyre to more productive subarctic waters (Fig. 1), regions with strong contrasts in macronutrient supply rates and phytoplankton community structure. To help interpret these data, we compared them with measurements and models of laboratory populations of diverse phytoplankton. Our findings support the hypotheses that the macromolecular composition of surface particulate matter underpins large-scale patterns in particulate C:N:P and reflects the acclimation of phytoplankton to changes in nutrient supply and growth rate.

Results and Discussion

Spatial Patterns in Environmental Conditions and Elemental Stoichiometry. In describing the spatial variation of particulate C:N:P and its drivers, we define three regions with distinct environmental conditions and phytoplankton communities: the NPSG as well as the southern and the northern regions of the North Pacific TZ (Fig. 1). The boundary between the NPSG and the STZ was defined by the 34.8 surface isohaline at ~32.8°N (32, 33) and the boundary between the STZ and the NTZ was delineated by the location of the 0.15 mg m⁻³ surface chlorophyll concentration at 36.2°N (34); the northern most extent of the NTZ was not reached on the transect. SST varied from ~27 °C in the NPSG to ~12 °C in the NTZ during the transect (Fig. 1). DIN and dissolved inorganic phosphorus (DIP) were <0.1 μM and <0.2 μM, respectively, in the NPSG and STZ and increased 2- to 20-fold within the NTZ. DIN:DIP was low (0.2 to 1.0) relative to the canonical Redfield N:P value of 16 throughout the transect except north of 39.5°N in the NTZ, where it increased to 1.9 to 4.3. In the NPSG, the picocyanobacterium *Prochlorococcus* was numerically dominant, while the picocyanobacterium *Synechococcus* and eukaryotic picophytoplankton were more abundant in the TZ (Fig. 1F). These patterns are broadly consistent with previous observations (35, 36) and the greater supply of macronutrients from upwelling, deeper winter convection, and Ekman transport in the TZ (37) that would promote larger eukaryotic phytoplankton (38, 39).

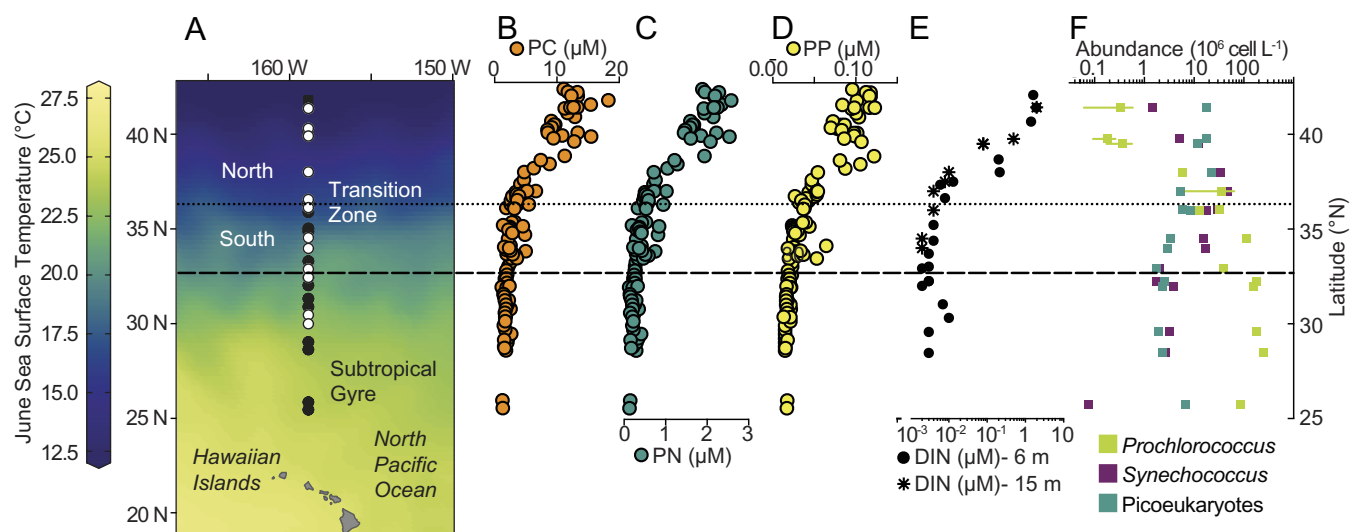


Fig. 1. (A) The mean sea surface temperature (SST) of the study area from 1955 to 2015 over the period of the cruise (27 May to 12 June), illustrating the environmental gradient spanning the North Pacific Subtropical Gyre (NPSG) and North Pacific TZ. Symbols on the map indicate major sampling points for the northbound (black) and southbound (white) portions of the cruise. Additional panels show the latitudinal variation in particulate carbon (B), particulate nitrogen (C), particulate phosphorus (D), dissolved inorganic nitrogen (DIN) (E), and community structure of phytoplankton $\leq 4 \mu\text{m}$ in estimated spherical diameter (F). The particulate element measurements represent 110 samples. The different symbols on panel E indicate samples collected by underway flow-through system at ~6 m depth (circle, $n = 15$) or by CTD-rosette at ~15 m depth (star, $n = 15$). Error bars in panel F indicate one SD among triplicate measurement at each discrete sample point ($n = 15$). The dashed line at 32.8°N delineates the subtropical gyre (NPSG) and TZ based on salinity while the dotted line at 36.2°N delineates the south transition zone (STZ) and north transition zone (NTZ) based on surface chlorophyll concentration (see *Results and Discussion* for regional boundary definitions).

Particulate C, N, and P concentrations increased sharply (~4.5- to sixfold) northward from the NPSG to the TZ (Fig. 1). This northward trend was superimposed over local variability that was relatively low in the NPSG, with particulate C and P displaying less variability (15.0 to 20.6%) than particulate N (31.3%) and increased (along with mean values) in the STZ (33.9 to 41.6%) and NTZ (37.9 to 48.8%) (Fig. 1). In addition, there was a clear trend of declining particulate C:N moving northward across the North Pacific gradient (Fig. 2). Particulate C:N had a strong negative relationship with latitude (Spearman's Rho = -0.69, $P < 0.001$) and was significantly higher within the oligotrophic NPSG (8.0 ± 1) than in the STZ (6.7 ± 0.9) and NTZ (6.1 ± 0.5) regions [$P < 0.001$, multivariate ANOVA (MANOVA) with Games-Howell post hoc tests; Fig. 2 and *SI Appendix, Table S2*]. This northward trend in C:N is consistent with the general subtropical-to-subpolar trend observed in recent global data compilations (4). In contrast, C:P and N:P of particulate matter were more variable (25.1 to 25.8%) than C:N (16.9%) and showed no significant relationship with latitude (Spearman's Rho = 0.02 to 0.16, $P = 0.02$ to 0.80) or significant difference among study regions ($P = 0.2$ to 0.8, MANOVA with Games-Howell post hoc tests; Fig. 2 and *SI Appendix, Table S2*).

Major Macromolecules Account for the Amount and Stoichiometry of Surface Particulate C, N, and P. To address the hypothesis that large-scale latitudinal variation in the C:N:P of particulate matter reflects its macromolecular composition, we measured the concentrations

of major macromolecular pools (protein, carbohydrate, lipid, DNA, RNA, pigments, and polyphosphate) across the North Pacific gradient. As with surface particulate C, N, and P, all the macromolecule concentrations increased with latitude to the north of the NPSG (*SI Appendix, Fig. S1*). The contribution of each macromolecule to particulate C, N, and P was calculated using their known elemental stoichiometry (9) or directly measured in the case of P content in phospholipids and polyphosphate. The majority of C, N, and P in surface particulate matter is accounted for by the contributions from these macromolecules. The summed elemental contents of these macromolecules contributed $90.1 \pm 11\%$ of particulate C, $76.7 \pm 15\%$ of particulate N, and $96.8 \pm 8\%$ of particulate P (*SI Appendix, Fig. S1*) when compared to the independent measurements of particulate C, N, and P (Fig. 1). The combined macromolecular elemental content also has a stoichiometry, a macromolecular C:N:P, that can be compared to the independently measured total particulate C:N:P (Fig. 2*A* and *B*). The macromolecular C:N shows a northward decline and strong negative relationship with latitude (Pearson's $R = -0.86$, $P < 0.001$) that closely matches the magnitude and direction of the trend in particulate C:N. However, macromolecular C:N values were generally higher than particulate C:N (10 ± 2 vs. 8.0 ± 1 , mean difference of 19.3%) largely due to the lower proportion of particulate N ($76.7 \pm 15\%$) accounted for by macromolecular measurements as compared to particulate C ($90.1 \pm 11\%$). As with total particulate stoichiometry, macromolecular C:P and N:P showed no clear latitudinal trend (Fig. 2*B* and *C*; Pearson's R , $P = 0.1$ to

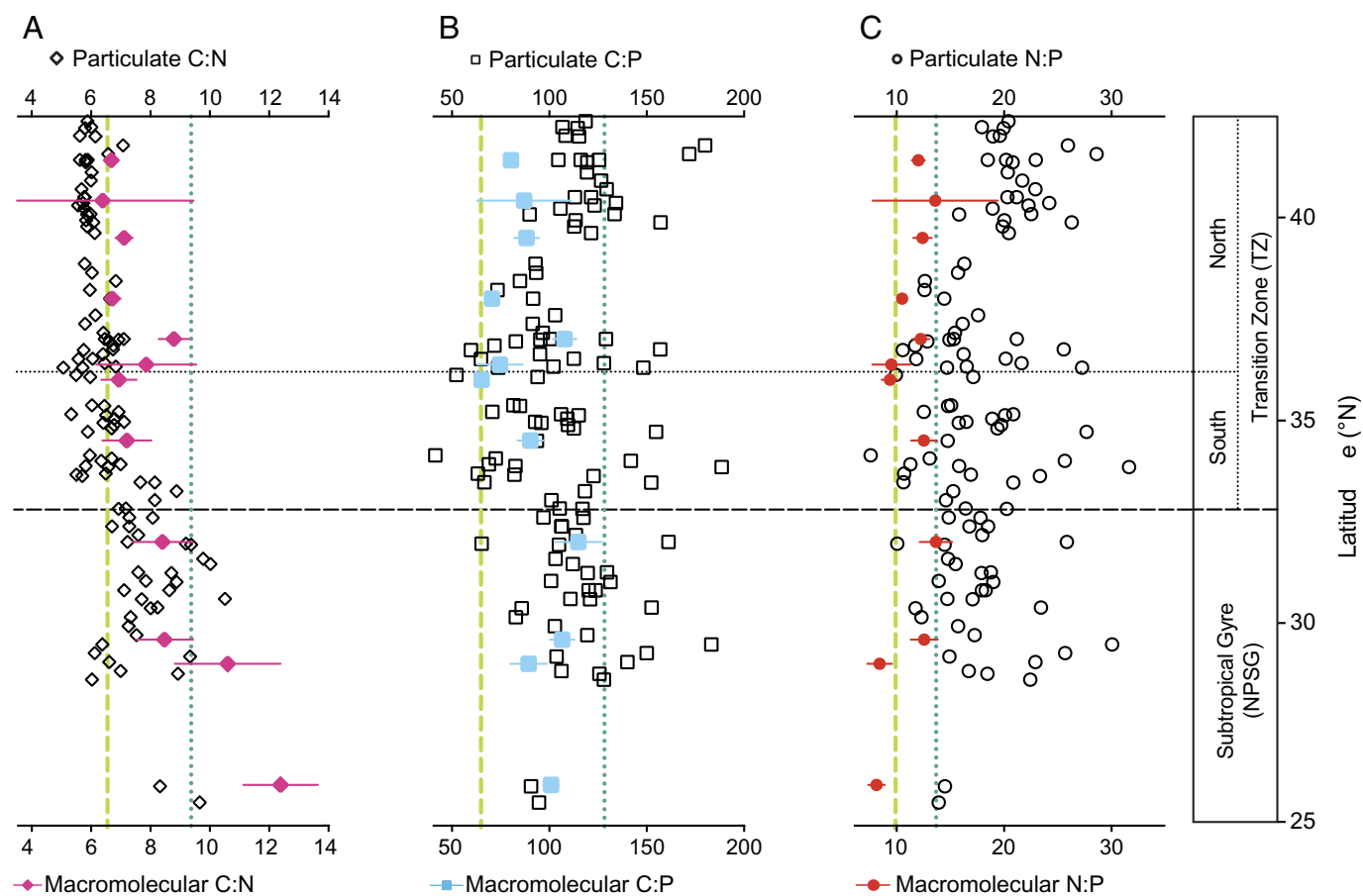


Fig. 2. Latitudinal variation in the macromolecular ($n = 12$) and total particulate ($n = 110$) molar ratio of (A) carbon:nitrogen, (B) carbon:phosphorus, and (C) nitrogen:phosphorus. Error bars for macromolecular ratios indicate one SD among replicate samples. The elemental contents of macromolecules in sampled particulate matter were calculated as described in *Materials and Methods* and in full detail in *SI Appendix*. The horizontal lines and inset of the vertical axis indicate the boundaries between the NPSG and the TZ (dashed line at 32.8°N) as well as the STZ and NTZ regions of the TZ (dotted line at 36.2°N). The vertical lines indicate the macromolecular elemental stoichiometry determined in N-starved cultures of *Prochlorococcus marinus* MED4 (cyan dotted lines), representative of the oligotrophic, picocyanobacteria-dominated NPSG, and nutrient-replete cultures of *Ostreococcus tauri* OTH95 (green dashed lines), representative of the more nutrient-rich, eukaryote-dominated NTZ.

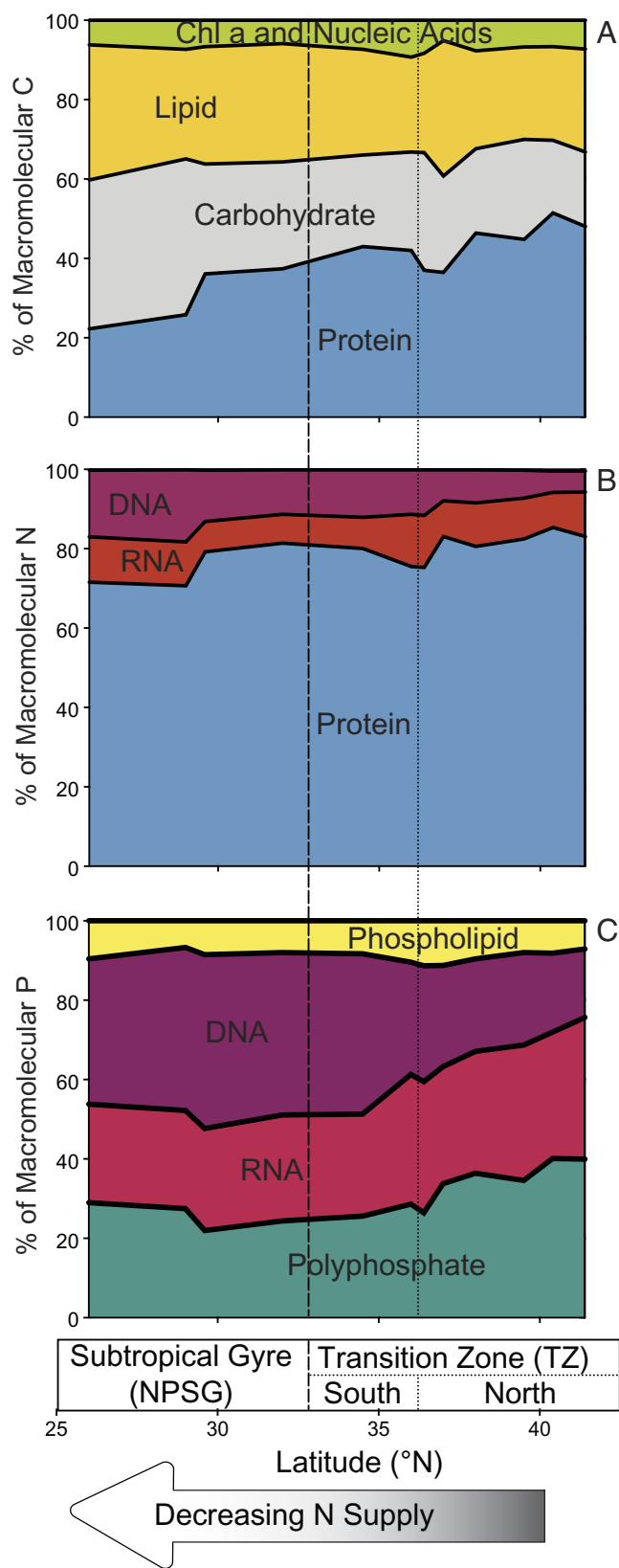


Fig. 3. The allocation (%) of macromolecular (A) carbon, (B) nitrogen, and (C) phosphorus among each macromolecular pool across the study area. Elemental contents of macromolecules were determined as described in the legend of Fig. 2 and *SI Appendix*. The error among replicate samples is not shown but was generally low (mean of 12% variation) and is shown in *SI Appendix*, Tables S6–S8. The arrow at the bottom of the figure indicates the decreasing nutrient supply and increasing N-limitation moving southward from the NTZ to the NPSG. The vertical lines and inset of the horizontal axis indicate regional boundaries.

0.2). Macromolecular C:P values were lower than (mean difference of 20.0%) but fell within the same range as particulate C:P values. Macromolecular N:P was considerably lower than particulate N:P (mean difference of 46.2%), which reflects the greater proportion of particulate P ($96.8 \pm 8\%$) accounted for in macromolecules and the higher overall variability in particulate C:P and N:P values (Fig. 2 *B* and *C* and *SI Appendix*, Table S2). The strengths and possible sources of error in our estimates of macromolecular contributions to particulate C:N:P are addressed further in *SI Appendix*.

The finding that C, N, and P content of intact macromolecules can be used to effectively reconstruct bulk particulate matter may be unexpected given that detritus has been estimated to comprise >50% of total particulate organic carbon (27–29) and the proportion of particulate matter that can be measured as macromolecules declines quickly with age (8). Yet organic detritus in the open ocean is ultimately derived from phytoplankton (40) and much of the detrital decomposition that would significantly alter macromolecular contents is thought to occur as particles sink out of the euphotic zone (41). Given that the composition of particulate matter we sampled is largely accounted for by measured macromolecules, we hypothesize that most of the detritus in the surface waters (i.e., at ~6 m depth) across the North Pacific gradient must be of recent planktonic origin and relatively unprocessed.

Variation in surface particulate C and N and its macromolecular basis across the transect was generally driven by changing protein content (Fig. 3 *A* and *B*). Protein represented the largest pool of total particulate C (19.2 to 42.9% of C) (*SI Appendix*, Table S3) and macromolecular C (22.3 to 51.5% of C) (Fig. 3*A*) along the transect except south of ~29°N in the NPSG, where contributions from carbohydrate ($33.8 \pm 5\%$), lipid ($31.7 \pm 5\%$), and protein ($31.7 \pm 10\%$) to particulate C were similar (*SI Appendix*, Table S3). Protein also accounted for the majority of total particulate N ($60.8 \pm 15\%$) (*SI Appendix*, Table S4) and macromolecular N ($79.4 \pm 14\%$) across the transect (Fig. 3*B*). The ~15-fold increase in N-rich protein from the NPSG to the NTZ, a greater increase than all other macromolecules (e.g., ~6-fold for carbohydrate and lipid) (*SI Appendix*, Fig. S2), explains the corresponding northward decline in particulate C:N across these regions (Fig. 2*A*).

The composition of macromolecules contributing to particulate P showed a clear shift across the North Pacific gradient (Fig. 3*C*) from DNA in the oligotrophic NPSG ($39.4 \pm 5\%$ of total particulate P) to RNA ($24.6 \pm 2\%$) and polyphosphate ($24.8 \pm 2\%$) in the NTZ (*SI Appendix*, Table S5). The contribution of phospholipids to particulate P was comparatively small and consistent ($8.4 \pm 2\%$) across the transect. Notably, we find that polyphosphate represents a major portion of surface particulate P across the transect (18.0 to 48.7% of P) and had the greatest spatial variation (12.7-fold) among P-rich macromolecules (*SI Appendix*, Table S5 and Fig. S2).

Potential Drivers of Macromolecular Variation and Particulate C:N:P. The macromolecules that largely determine surface particulate C:N:P also play specific functional roles in their living sources and provide a bridge to mechanistic interpretation and modeling of large-scale elemental patterns. Large-scale variations in ocean particulate C:N:P have been attributed to changes in phytoplankton community composition (5, 14) and the acclimation of phytoplankton cell contents to environmental conditions (5, 6, 21). The relative contribution of heterotrophic zooplankton and bacteria to particulate matter (25, 42, 43) or the contribution of detritus and its alteration by heterotrophs (31) have also been suggested to regulate particulate C:N:P. To evaluate these potential controls, we estimated the abundance and cell size

of living phytoplankton and heterotrophic plankton using flow cytometry and cell imaging and then calculated their contribution to particulate carbon using published group-specific carbon to volume relationships (*SI Appendix, Table S9*). Phytoplankton biomass represents an estimated $32.90 \pm 2.2\%$ of particulate C across the transect with smaller contributions from heterotrophic bacteria ($8.5 \pm 8\%$) and heterotrophic protists ($1.47 \pm 1.0\%$) for a total contribution of $42.9 \pm 8\%$ to particulate C by intact plankton. While these conservative estimates for the contribution of heterotrophic bacteria have large uncertainties, they are comparable to previous estimates of $6.8 \pm 1.1\%$ in the NPSG (44) and ~ 8 to 14% in analogous laboratory studies (31). Additionally, our estimated contribution of intact plankton to particulate C falls between previous estimates for the contribution of living plankton to particulate C of 29.8% in the NPSG (45) and $60 \pm 17\%$ in other ocean regions (5). The remaining particulate material is in either living zooplankton or organic detritus. In lieu of direct measurements, we can estimate the contribution of zooplankton from its typical power law relationship with phytoplankton biomass (46), which yields a zooplankton:phytoplankton biomass ratio (Z:P) of ~ 0.8 to 2.5 in open ocean settings, with the higher ratios associated with lower phytoplankton biomass. In combination with our estimates of phytoplankton and heterotrophic bacteria biomass, this Z:P relationship implies a $\geq 26\%$ contribution of zooplankton to particulate carbon and a complementary detrital contribution of $\leq 31\%$.

Our data indicate that living phytoplankton biomass contributes approximately a third of the total particulate carbon along the transect, directly affecting elemental and macromolecular ratios and indirectly affecting these ratios as a source of detritus. The observed northward decline in C:N reflects a greater increase in the N-rich protein content of particulate matter relative to C-rich carbohydrate and lipid (Fig. 3 *A* and *B*). To what extent might this shift in C:N be driven by the community composition or physiological acclimation of phytoplankton? Considering community composition, we note that the strongest evidence for its influence on C:N:P across ocean regions pertains to C:P and N:P (6, 14, 47) while its impact on large-scale C:N patterns are comparatively small (48). Likewise, culture studies show much greater taxonomic variability in C:P and N:P among major phytoplankton taxa than is observed for C:N (10, 11). The largest phylogenetic differences in C:N are found between eukaryotic phytoplankton and cyanobacteria, with the latter having greater steady-state protein content and subsequently lower C:N (12). Cell size may also affect variation in C:N among phytoplankton communities since the overall size-scaling exponent for protein is less than 1 and considerably lower than that of carbohydrate (49), indicating that relative protein content will decline and C:N will increase as cell size increases. Considering these taxonomic and allometric patterns, the northward shift in dominance from picocyanobacteria to larger eukaryotes (Fig. 1*F*) along the North Pacific gradient would be expected to drive a northward decline in relative protein content and corresponding increase in C:N, which is in opposition to the trends we observed.

The northward decline in C:N and shift in community composition along the transect were also accompanied by a steep gradient of increasing nutrient supply. Incubation experiments revealed nitrogen to be the primary limiting resource in the NPSG during this study (50) and fixed nitrogen concentrations increased sharply in the TZ (Fig. 1*E*). In phytoplankton cultures, C:N varies by a factor of 3 in response to steady-state N-limitation (17–19) as N-rich protein quotas decline in order to lower N demand while fixed carbon accumulates due to slower N-limited growth rate. Lower light intensity and higher growth rates lead to higher investments in photosynthetic and biosynthetic proteins respectively

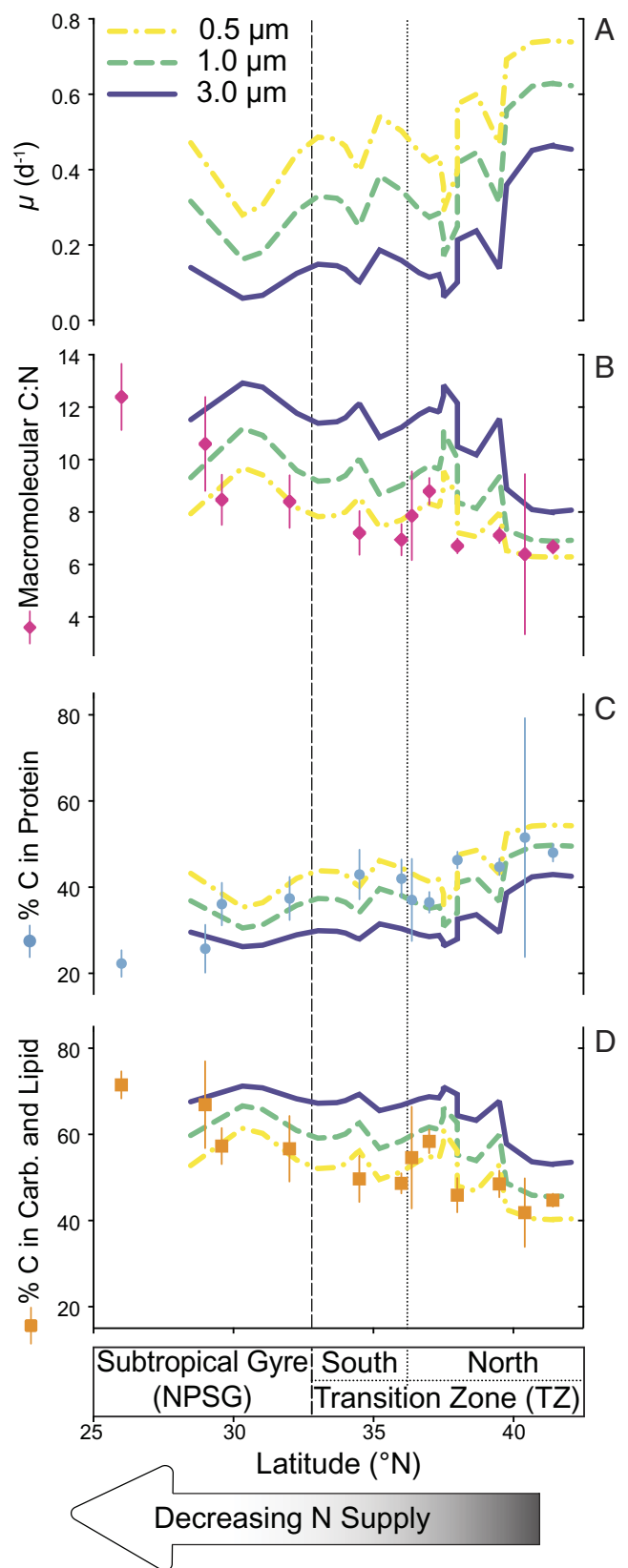


Fig. 4. The predicted growth rate (*A*), macromolecular C:N (*B*), and proportion (%) of macromolecular C found in (*C*) protein as well as the (*D*) the sum of carbohydrate and lipid for phytoplankton size classes of 0.5, 1.0, and 3.0 μm equivalent spherical diameter (solid and dashed lines). Observed values of macromolecular elemental stoichiometry and contribution to macromolecular C are shown as discrete symbols in panels *B–D* for comparison ($n = 12$). Error bars indicate one SD among duplicate (%C in Carb. and Lipid) or triplicate (%C in Protein) samples. The vertical lines and inset of the horizontal axis indicate regional boundaries.

(9, 23, 51) and thus a reduction in C:N (52). These relationships have been quantitatively encapsulated in an allocation-based model of phytoplankton cell composition (53). Driving the model with estimates of N-limited growth rate based on allometric relationships and observed nutrient concentrations (*Materials and Methods*) we predicted the acclimated macromolecular and elemental composition of phytoplankton along the transect for cell size classes of 0.5 μm , 1.0 μm , and 3.0 μm (Fig. 4 and *SI Appendix, Figs. S3 and S4*), which are largely representative of the community as we estimate that cells $<4 \mu\text{m}$ are $65.7 \pm 10\%$ of phytoplankton biomass (*SI Appendix, Table S9*). Under N-depleted conditions, growth rates are slow and excess photosynthate is allocated to carbohydrate and/or lipid storage (54, 55). As N availability and growth rate increase northward (Fig. 4A), the predicted macromolecular C:N declines due to increased protein content for biosynthesis and less accumulation of carbohydrate and lipid as fixed C is diverted from storage to cell growth. The model predictions are broadly consistent with the observed trends in C:N (Fig. 4B) and the relative contributions of protein, carbohydrate, and lipid to particulate matter (Fig. 4 C and D and *SI Appendix, Fig. S3*), supporting the notion that understanding phytoplankton acclimation is key to developing predictive and interpretive models of ocean stoichiometry. Although the model captures the overall trend in C:N and its macromolecular basis, the observed northward shift from carbohydrates and lipids to protein is of greater magnitude than predicted (Fig. 4 and *SI Appendix, Fig. S3*) and not dampened by a northward increase in phytoplankton cell size (Fig. 1) as the model would suggest. Model predictions for the relative contribution of N- and P-rich macromolecules are also broadly consistent with our observations (*SI Appendix, Figs. S3 and S4*), but macromolecular C:P and N:P are overestimated across the study area (*SI Appendix, Fig. S4*) due to underestimates in per carbon and per nitrogen content of RNA, DNA, and polyphosphates. This might reflect the model calibration being primarily based on a single laboratory study (18, 53) that may not be representative of the whole community. This discrepancy highlights the value of laboratory or field studies (*SI Appendix, Table S1*) measuring the total content of these P-rich macromolecules and the need for more such measurements to constrain mechanistic models of ocean C:N:P.

While other environmental factors affecting phytoplankton growth and acclimation varied along the North Pacific gradient, their effects on phytoplankton C:N were likely minimal compared to the effects of N availability. The northward increase in N availability along the gradient is accompanied by an increase in P availability, while Fe availability shows a more complex northward pattern as it declines within the NPSG, increases in the STZ, and declines again in the subpolar NTZ (21, 50, 56). In addition to the pattern in Fe availability not aligning with the observed pattern in C:N (Fig. 2), the effects of P or Fe availability on phytoplankton C:N and its macromolecular basis appear too small to explain the observed northward decline in C:N (52). Variation in temperature like that observed along the gradient (~ 12 to 27°C) has been implicated in global C:P and N:P variability due to a decline in P-rich ribosome content in phytoplankton as translation efficiency increases with temperature (21, 48). Yet temperature appears to have little or no effect on the variability of C:N in surface particulate matter across ocean regions (48) or in phytoplankton cultures (52). In contrast, N availability has a considerably larger impact on phytoplankton C:N (17–19, 52) that better corresponds to the magnitude of C:N variation observed along the gradient. To compare the stoichiometric variation that we observed in the North Pacific with the acclimation of phytoplankton to N availability, we measured elemental and macromolecular composition in N-replete and N-starved batch cultures

of the picocyanobacterium *Prochlorococcus marinus* MED4, representative of phytoplankton in the oligotrophic NPSG, and the prasinophyte *Ostreococcus tauri*, which is representative of the picoeukaryote-dominated and nutrient-rich TZ regions. As with our field observations, the macromolecular composition of both cultured species accounted for the vast majority of their particulate C, N, and P content ($89.6 \pm 17\%$). The macromolecular allocation of C and N in the more productive NTZ region (Fig. 3 A and B) closely resembles that of both cultured species during N-replete (fast-growing) conditions (*SI Appendix, Fig. S5*). Likewise, C and N allocation in the oligotrophic NPSG is similar to that of both cultures during N-starvation (slow, or no-growth) except for the greater allocation of N to DNA in the NPSG (Fig. 3B and *SI Appendix, Fig. S5*) that may reflect slower degradation of detrital DNA when compared to RNA or protein (57). These parallels in cell composition result in a similar macromolecular C:N between N-starved *P. marinus* MED4 (9.4 ± 0.5) and the oligotrophic NPSG (9.9 ± 0.7) and between N-replete *O. tauri* ($6.6 \pm 0.1\%$) and the nutrient-rich NTZ ($7.1 \pm 1\%$) (Fig. 2B). While macromolecular C:P and N:P are also similar among the field samples and representative cultures (Fig. 2 B and C), the contributions of DNA and polyphosphate storage to these elemental ratios differ in all three instances (Fig. 3C and *SI Appendix, Fig. S5*). This variability and uncertainty in phytoplankton P content is also shown in our model predictions, which reproduced the observed trends in C:N, protein, carbohydrate, and lipid but were less accurate in predicting the contributions of DNA, RNA, and polyphosphate (*SI Appendix, Figs. S3 and S4*). These differences among observations and predictions of P allocation may reflect the lower P availability in the N-limited North Pacific compared to the cultures used in this study or those constraining the model (18, 53). These differences may also reflect the high phylogenetic variability in P content among phytoplankton (5, 10, 11) particularly when growth is limited by N, but not P (55).

Although living phytoplankton accounted for approximately a third of the biomass along the North Pacific gradient, the impact of the potentially similar amount of zooplankton biomass on the observed trend in particulate C:N should also be considered. Yet expected patterns in their relative contribution to particulate matter or the flexibility of their stoichiometry suggest that zooplankton are unlikely to drive the northward decline in C:N we observed. Metazoans that often dominate zooplankton (e.g. copepods) would likely contribute a consistently low C:N (~ 4.5 to 6) to particulate matter, even when the C:N of their prey is high (42, 58, 59). However, empirical allometric scaling across a wide range of marine environments suggests that the total zooplankton to phytoplankton biomass ratio (Z:P) would decline as phytoplankton productivity and biomass increase (46). These empirical relationships indicate that when moving northward from the NPSG to the more productive NTZ region, the relative contribution of low C:N zooplankton to sampled particulate material would decrease and thus be unlikely to cause the northward decline in particulate C:N. Heterotrophic protists within zooplankton communities have a more flexible C:N that is typically higher when prey is abundant and C reserves accumulate, and a lower C:N during starvation when C reserves are depleted (60, 61). Thus, heterotrophic protists would likely decrease C:N in the less-productive NPSG and increase C:N in the prey-rich NTZ (25), which opposes the observed trend in particulate C:N.

In short, the observed variation in particulate C:N and its underlying macromolecular composition along the North Pacific gradient are consistent in direction and magnitude with physiological acclimation of phytoplankton to nitrogen availability in an N-limited regime. The accompanying trends in phytoplankton community composition and expected elemental contribution of

zooplankton would likely drive an opposing trend, while other factors that affect phytoplankton acclimation (i.e. temperature and P availability) have little effect on particulate C:N (48, 52).

The Dynamic Macromolecular Basis of Particulate P. Although we did not find a clear latitudinal trend in C:P or N:P along the North Pacific gradient (Fig. 3C), we observed a shift in the relative composition of P-rich macromolecules that may provide insight into the mechanisms affecting C:P and N:P in other regions or at larger scales. The northward shift from DNA to RNA and polyphosphate as the major sources of particulate P could be attributed to a difference in detrital turnover rates across the gradient since RNA and polyphosphate are more labile than DNA (57, 62). Another explanation for this latitudinal shift that is better supported by the available data is that it reflects phytoplankton responses to increasing growth rate and P availability. A relative increase in RNA-rich biosynthetic components (i.e., ribosomes) would be expected as growth rates increase (23, 63) in the more productive TZ region. Similarly, the relative increase in polyphosphate could represent luxury uptake as P availability increases (16, 64). The northward decline in picocyanobacteria and increase in eukaryotes within the TZ could also contribute to spatial gradients in P allocation. Picocyanobacteria like *Synechococcus* have a lower RNA:DNA ratio that is less responsive to growth conditions (65, 66) when compared to eukaryotic phytoplankton (55), making the increase in RNA allocation along the transect consistent with the observed taxonomic shift. A shift to larger eukaryotic phytoplankton with a greater nutrient storage capacity (38) could also explain the northward increase in P allocation to polyphosphate storage. These corresponding trends in phytoplankton taxa, RNA, and polyphosphate provide a macromolecular basis for the hypothesis that global ocean patterns of C:P and N:P are driven by the biogeography of major phytoplankton taxa and their intrinsic differences in realized P storage and overall P content (3, 14).

Summary and Outlook. Our study gives strong support to the hypothesis that gyre- to basin-scale variations in the elemental (C:N:P) stoichiometry of surface ocean particulate matter corresponds to variations in six major classes of macromolecules: protein, carbohydrate, lipid, nucleic acids, polyphosphate, and pigment. Though our data span a major transition between subpolar and subtropical regimes and thousands of kilometers, future complementary datasets spanning other regimes would improve the quantitative link between particulate C:N:P and its biochemical basis. Similarly, the large-scale patterns we observed in C:N:P were superimposed on strong local variations that could not be compared to macromolecular measurements that were made less frequently. A corollary hypothesis is that the close relationship between elemental and macromolecular composition should hold across a range of spatial and temporal scales in the surface ocean, which could be investigated with a different sampling strategy. Our analysis indicated that nearly half of surface particulate matter consists of living phytoplankton as well as heterotrophic bacteria and protists, with the rest partitioned between zooplankton and detritus that originate from all of the above. The relative increase in protein and corresponding decline in C:N along the North Pacific gradient is unlikely to be driven by changes in phytoplankton community structure or the relative contribution of heterotrophs or detritus to particulate matter. Instead, the observed shift in C:N among ocean regions is consistent with the acclimation of phytoplankton to greater N supply and faster growth rates and is consistent with expectations based on laboratory cultures and empirically constrained models of phytoplankton acclimation. This provides a clear interpretation of the predominant basin-scale trend

in particulate C:N:P in this region and support for acclimation-based approaches in biogeochemical models. However, since phytoplankton directly account for only a third of the particulate matter sampled, this interpretation requires investigation. A more complete, quantitative partitioning of surface particulate matter into major trophic classes (phytoplankton, heterotrophic bacteria, zooplankton, and detritus) would be helpful. Characterizing the small portion of particulate matter that is not accounted for by major macromolecules would also help in understanding the drivers of surface particulate C:N:P patterns. In the meantime, acclimation models of macromolecular composition are a promising tool for predictive and mechanistic simulations of ocean particulate matter.

Materials and Methods

Elemental and Macromolecular Composition. Field data were collected between May 29th and June 12th, 2017 aboard the R/V *Marcus G. Langseth* following a latitudinal gradient along 158°W from ~25°N to a northernmost latitude of 42.38°N. Discrete samples for dissolved inorganic nutrients were collected from an uncontaminated underway flow-through system with a seawater intake located at ~6 m depth near the bow of the vessel ($n = 15$) and on station via CTD-rosette ($n = 15$ samples from ~15 m depth). Seawater collected by the underway flow-through system passed through a coarse screen (~500 μm) while seawater from the CTD-rosette was collected via Tygon tubing with an in-line 202 μm Nitex mesh. All samples were analyzed for nitrate plus nitrite (N + N) (67) and soluble reactive phosphorus (SRP, dominantly as phosphate) (68) using a segmented flow SEAL AutoAnalyzer 3 (69). The average precision for N + N and SRP was 0.4% and 0.2%, respectively. Accuracy, determined using Wako CSK certified reference standard solutions, was within 2%. For low concentrations (<0.5 μM), N + N concentrations were determined with a high sensitivity chemiluminescent method (70) with a detection limit of 1 nM and a precision ranging between 0.4% at 1,000 nM and 7% at 2 nM.

Particulate elemental samples were collected on precombusted (4.5 h at 450 °C) Whatman GF/F filters from the ship's underway flow-through system using semiautomated filtration systems (SAFS) (71) and described in detail in Supporting Information. Particulate C and N were analyzed on a CHNS analyzer (Carlo Erba, model NA1500) using cystine as the primary standard. Particulate P was analyzed after combustion and extraction (72) via molybdenum blue spectrophotometry (67) and quantified using certified reference material (National Institute of Standards, NIST 1515). Sensitivity, accuracy, and additional details regarding particulate elemental analyses are provided in *SI Appendix*. Variation in the molar stoichiometry (C:N, C:P, N:P) of these particulate elements was compared among the previously defined regions within the transect (32–34): the NPSG as well as the southern and the northern regions of the North Pacific Transition Zone (STZ and NTZ, respectively) (Fig. 1). Particulate elemental ratios were compared between regions using a MANOVA (73) with Games-Howell tests used for multiple comparisons and their relationship with latitude was examined with Spearman's rank correlation (73) due to uneven sample size and variance among regions. Macromolecular elemental ratios were not compared categorically between regions due to their small and uneven sample size, but their relationship with latitude was examined with a Pearson's correlation (73).

Surface water samples for macromolecular content were collected from the ship's underway flowthrough system between the hours of ~05:00 and 14:00 local time at 12 stations. Vacuum filtration under gentle pressure (<18 kPa) and low light was used to collect samples for protein (in triplicate), carbohydrate, RNA, and DNA (in duplicate) on 47 mm polycarbonate filters with a 0.2 μm pore size (Whatman Nuclepore). Triplicate samples for lipid, polyphosphate, and chlorophyll *a* were collected in the same fashion except using precombusted (4 h at 450 °C) 47 mm GF/F filters (Whatman). Both filter types have been shown to collect the smallest phytoplankton (i.e., *Prochlorococcus*) similarly (74), as well as ~50 to 90% of heterotrophic bacteria present (75, 76). Samples were immediately frozen with liquid nitrogen and stored at –80 °C or on dry ice (during shipment) until analysis.

All macromolecule samples were freeze-dried prior to analysis. Protein samples were extracted by bead-milling in lysis buffer (77) and quantified with the Pierce BCA Protein assay (Thermo Fisher Scientific). Polyphosphate was extracted

with a neutral phenol/chloroform mixture followed by nuclease treatment to destroy RNA and DNA and then purified by ethanol precipitation (78). Purified polyphosphate was then enzymatically hydrolyzed with acid phosphatase (Sigma-Aldrich, #P1146) (62) and quantified as orthophosphate (79). Chlorophyll *a* and divinyl-chlorophyll *a* were extracted in 90% acetone:DMSO (80) and measured with a Turner AU-10 fluorometer against a chlorophyll *a* standard (Sigma-Aldrich, #96145). Analyses of carbohydrate, lipid, RNA, and DNA were performed as described in Liefer et al. (55) with the exception that extracted carbohydrates were quantified with a modified phenol-sulfuric acid method (81). The elemental contents of measured macromolecules were calculated from their elemental stoichiometry, which was based on their single molecular structure (chlorophyll *a*, divinyl-chlorophyll *a*), on published mean values (carbohydrate, lipid, protein, nucleic acids), or measured directly in the case of P content in phospholipids and polyphosphate (see *SI Appendix* for full description of the elemental accounting in macromolecules).

Plankton Community Composition and Contribution to Particulate Matter. Samples for the abundance and biovolume of surface phytoplankton were collected with an underway flow-through system connected to two flow cytometers. Picophytoplankton (0.4 to 4 μm) were measured with a SeaFlow flow cytometer (82) and categorized as *Prochlorococcus*, *Synechococcus*, or picoeukaryotes based on fluorescence properties and equivalent spherical diameter estimated by Mie light-scattering theory (83). Phytoplankton and heterotrophic protists (4 to 100 μm in diameter) were enumerated with an Imaging FlowCytobot (IFCB; McLane Research Laboratories) and their biovolume was calculated from collected images using a known pixel: μm ratio and a distance map algorithm (84). Discrete samples for the abundance of surface heterotrophic bacteria were collected by CTD-rosette ($n = 15$ samples from ~15 m depth) from 30 to 42°N, fixed in glutaraldehyde (0.01% vol/vol), flash frozen, stained with SYBR Green I dye (Lonza Bioscience, #50513) and measured with an Influx flow cytometer (Becton-Dickinson) based on forward light scatter, SYBR Green I fluorescence, and lack of chlorophyll fluorescence. Estimated biovolumes from SeaFlow and IFCB samples were converted to cellular carbon quotas based on empirical, group-specific allometric relationships (85), while a carbon quota of 10 fg C cell⁻¹ was assumed for heterotrophic bacteria (86). Biomass estimates (as carbon) for plankton and particulate organic carbon (POC) were averaged in 1° latitude bins to estimate the bulk contribution of each planktonic group (% of total POC) to surface particulate matter (*SI Appendix, Table S9*). Additional discrete samples for picophytoplankton (*Prochlorococcus*, *Synechococcus*, and picoeukaryotes) were collected on station via CTD-rosette ($n = 15$ samples from 15 m depth) and measured with an Influx flow cytometer, providing comparable measurements as those made with the SeaFlow. These discrete picophytoplankton measurements are shown in Fig. 1A to summarize overall community composition trends. A more detailed description of flow cytometry methods and group-specific biomass estimates are provided in *SI Appendix*.

Laboratory Phytoplankton Cultures. Axenic *P. marinus* MED4 (CCMP 2389) was obtained from the National Center for Marine Algae and Microbiota (NCMA) and *O. tauri* (OTH95, RCC745) was obtained from the Roscoff Culture Collection (RCC). Triplicate cultures of each strain were sampled during nutrient-replete, balanced exponential growth and during the onset of N-starvation. Culturing methods as well as sampling and analysis for particulate elements (C, N, and

P) and macromolecules were the same as in Liefer et al. (55) with minor modifications for culturing of *P. marinus* MED4 and filter types used for sampling (*SI Appendix*).

Allocation Model. We modeled the macromolecular acclimation and allocation of phytoplankton (Fig. 4 and *SI Appendix, Figs. S3 and S4*) following Inomura et al. (53) with distinct model estimates for three cell size classes (0.5, 1.0, and 3.0 μm) that are broadly representative of the overall phytoplankton community in the study area. Under N-limited conditions, all cellular C, N, and P are allocated to protein, carbohydrates, lipids, DNA, RNA, chlorophyll *a*, and polyphosphate, each with empirically fixed elemental composition. Protein is allocated among the functional pools of light harvesting, biosynthesis and a fixed “essential” pool and other macromolecular and protein allocation parameters are constrained by laboratory data (53) (*SI Appendix*). Inputs for the model are growth rate and light intensity. We estimated growth rates as the nitrogen-specific, nitrogen uptake rate, informed by empirical allometric relationships (87) and assumed that light intensity was saturating at 6 m depth and 12 h:12 h light:dark cycle. As an extension of the Inomura et al. model (53), we assumed phytoplankton polyphosphate content was equal to RNA content under N-limitation based on an empirical interpretation (64). Lipids and carbohydrates were treated as a single pool and, for the purposes of display, shown as equal in magnitude. We did not include the explicit representation of carbon in thylakoid phospholipids. Also, we assumed a constant C fraction of DNA 1.91×10^{-2} (molC molC⁻¹) based on the *P. marinus* MED4 culture data from this study.

Data, Materials, and Software Availability. All particulate elemental and macromolecular data in this study are included in the article and in the *SI Appendix*. Field data for particulate elements (88), particulate macromolecules (89), and plankton community composition (90–92) have been deposited and are publicly accessible on Zenodo (<http://Zenodo.org>) and also available through the Simons Collaborative Marine Atlas Project (<https://simonscm.com>), with dataset names provided in the *SI Appendix*.

ACKNOWLEDGMENTS. This research was supported by the Simons Foundation through the Simons Collaboration on Ocean Processes and Ecology (Award No. 426570SP to A.E.W., E.V.A., D.M.K., and M.J.F., and Award No. 721566 to A.E.W.), the Simons Collaboration on Computational Biogeochemical Modeling of Marine Ecosystems (Awards 549937 to Z.V.F., 549935 to A.J.I., and 549931 to M.J.F.) and a Simons Postdoctoral Fellowship in Marine Microbial Ecology (Award 544338 to K.I.). Funding was also provided by the Natural Sciences and Engineering Research Council of Canada and the Canada Research Chairs program (Z.V.F.). We thank Rosie Sheward for contributing the map image in Fig. 1 and insight into figure design. We thank Sara Ferrón for providing dissolved inorganic nutrient analyses.

Author affiliations: ^aDepartment of Biology, Mount Allison University, Sackville, NB E4L 1G7, Canada; ^bDepartment of Oceanography, University of Hawai‘i at Mānoa, Honolulu, HI 96822; ^cDepartment of Oceanography, Dalhousie University, Halifax, NS B3H 4R2, Canada; ^dDepartment of Mathematics and Statistics, Dalhousie University, Halifax, NS B3H 4R2, Canada; ^eGraduate School of Oceanography, University of Rhode Island, Kingston, RI 02881; ^fSchool of Oceanography, University of Washington, Seattle, WA 98195; ^gDepartment of Geography and Environment, Mount Allison University, Sackville, NB E4L 1G7, Canada; and ^hDepartment of Earth, Atmospheric, and Planetary Science, Massachusetts Institute of Technology, Cambridge, MA 02139

1. T. Volk, M. I. Hoffert, “Ocean carbon pumps: Analysis of relative strengths and efficiencies in ocean-driven atmospheric CO₂ changes” in *The Carbon Cycle and Atmospheric CO₂: Natural Variations Archaean to Present*, E. T. Sundquist, W. S. Broecker, Eds. (American Geophysical Union, 1985), pp. 99–110.
2. A. C. Redfield, The biological control of chemical factors in the environment. *Am. Sci.* **46**, 205–221 (1958).
3. T. S. Weber, C. Deutsch, Ocean nutrient ratios governed by plankton biogeography. *Nature* **467**, 550 (2010).
4. A. C. Martiny, J. A. Vrugt, F. W. Primeau, M. W. Lomas, Regional variation in the particulate organic carbon to nitrogen ratio in the surface ocean. *Global Biogeochem. Cycles* **27**, 723–731 (2013).
5. A. C. Martiny et al., Strong latitudinal patterns in the elemental ratios of marine plankton and organic matter. *Nat. Geosci.* **6**, 279–283 (2013).
6. E. D. Galbraith, A. C. Martiny, A simple nutrient-dependence mechanism for predicting the stoichiometry of marine ecosystems. *Proc. Natl. Acad. Sci. U.S.A.* **112**, 8199–8204 (2015).
7. L. Kwiatkowski, O. Aumont, L. Bopp, P. Ciais, The impact of variable phytoplankton stoichiometry on projections of primary production, food quality and carbon uptake in the global ocean. *Global Biogeochem. Cycles* **32**, 516–528 (2018).
8. S. G. Wakeham, C. Lee, J. I. Hedges, P. J. Hernes, M. J. Peterson, Molecular indicators of diagenetic status in marine organic matter. *Geochim. Cosmochim. Acta* **61**, 5363–5369 (1997).
9. R. J. Geider, J. LaRoche, Redfield revisited: Variability of C:N:P in marine microalgae and its biochemical basis. *Eur. J. Phycol.* **37**, 1–17 (2002).
10. A. Quigg et al., The evolutionary inheritance of elemental stoichiometry in marine phytoplankton. *Nature* **425**, 291–294 (2003).
11. N. S. Garcia et al., High variability in cellular stoichiometry of carbon, nitrogen, and phosphorus within classes of marine eukaryotic phytoplankton under sufficient nutrient conditions. *Front. Microbiol.* **9**, 543 (2018).
12. Z. V. Finkel et al., Phylogenetic diversity in the macromolecular composition of microalgae. *PLoS ONE* **11**, e0155977 (2016).

13. J. A. Bonachela, C. A. Klausmeier, K. F. Edwards, E. Litchman, S. A. Levin, The role of phytoplankton diversity in the emergent oceanic stoichiometry. *J. Plankton Res.* **38**, 1021–1035 (2016).
14. S. Sharoni, I. Halevy, Nutrient ratios in marine particulate organic matter are predicted by the population structure of well-adapted phytoplankton. *Sci. Adv.* **6**, eaaw9371 (2020).
15. M. Droop, The nutrient status of algal cells in continuous culture. *J. Mar. Biol. Assoc. U.K.* **54**, 825–855 (1974).
16. A. Moreno, A. Martiny, Ecological stoichiometry of ocean plankton. *Annu. Rev. Mar. Sci.* **10**, 43–69 (2017).
17. I. R. Elfrin, D. H. Turpin, Steady-state luxury consumption and the concept of optimum nutrient ratios: A study with phosphate and nitrate limited *Selenastrum minutum* (Chlorophyta). *J. Phycol.* **21**, 592–602 (1985).
18. F. P. Healey, Interacting effects of light and nutrient limitation on the growth rate of *Synechococcus linearis* (Cyanophyceae). *J. Phycol.* **21**, 134–146 (1985).
19. N. Leonardos, R. J. Geider, Responses of elemental and biochemical composition of *Chaetoceros muelleri* to growth under varying light and nitrate:phosphate supply ratios and their influence on critical N:P. *Limnol. Oceanogr.* **49**, 2105–2114 (2004).
20. K. L. Terry, J. Hirata, E. A. Laws, Light-, nitrogen-, and phosphorus-limited growth of *Phaeodactylum tricornutum* Bohlin strain TFX-1: Chemical composition, carbon partitioning, and the diel periodicity of physiological processes. *J. Exp. Mar. Biol. Ecol.* **86**, 85–100 (1985).
21. A. Toseland *et al.*, The impact of temperature on marine phytoplankton resource allocation and metabolism. *Nat. Clim. Change* **3**, 979–984 (2013).
22. F. C. García, E. Bestion, R. Warfield, G. Yvon-Durocher, Changes in temperature alter the relationship between biodiversity and ecosystem functioning. *Proc. Natl. Acad. Sci. U.S.A.* **115**, 10989–10994 (2018).
23. R. W. Sterner, J. J. Elser, *Ecological Stoichiometry: The Biology of Elements from Molecules to the Biosphere* (Princeton University Press, 2002).
24. A. E. Zimmerman, S. D. Allison, A. C. Martiny, Phylogenetic constraints on elemental stoichiometry and resource allocation in heterotrophic marine bacteria. *Environ. Microbiol.* **16**, 1398–1410 (2014).
25. D. Talmy, A. Martiny, C. Hill, A. Hickman, M. Follows, Microzooplankton regulation of surface ocean POC:PON ratios. *Global Biogeochem. Cycles* **30**, 311–332 (2016).
26. N. Jiao *et al.*, Microbial production of recalcitrant dissolved organic matter: Long-term carbon storage in the global ocean. *Nat. Rev. Microbiol.* **8**, 593–599 (2010).
27. D. W. Menzel, J. J. Goering, The distribution of organic detritus in the ocean. *Limnol. Oceanogr.* **11**, 333–337 (1966).
28. J. R. Christian, D. M. Karl, Microbial community structure at the US-Joint Global Ocean Flux Study Station ALOHA: Inverse methods for estimating biochemical indicator ratios. *J. Geophys. Res. Oceans* **99**, 14269–14276 (1994).
29. D. Caron *et al.*, The contribution of microorganisms to particulate carbon and nitrogen in surface waters of the Sargasso Sea near Bermuda. *Deep-Sea Res. I, Oceanogr. Res. Pap.* **42**, 943–972 (1995).
30. D. M. Karl, F. C. Dobbs, "Molecular approaches to microbial biomass estimation in the sea" in *Molecular Approaches to the Study of the Ocean*, K. E. Cooksey, Ed. (Springer, 1998), pp. 29–89.
31. P. Verity, S. Williams, Y. Hong, Formation, degradation, and mass: Volume ratios of detritus derived from decaying phytoplankton. *Mar. Ecol. Prog. Ser.* **207**, 53–68 (2000).
32. G. I. Roden, "Subarctic-subtropical transition zone of the North Pacific: Large-scale aspects and mesoscale structure" in *NOAA technical report NMFS 105-Biology, Oceanography, and Fisheries of the North Pacific Transition Zone and Subarctic Frontal Zone*, J. A. Weatherall, Ed. (1991), pp. 1–38.
33. M. R. Gradoville *et al.*, Latitudinal constraints on the abundance and activity of the cyanobacterium UCMY-A and other marine diazotrophs in the North Pacific. *Limnol. Oceanogr.* **65**, 1858–1875 (2020).
34. C. L. Follett, S. Dutkiewicz, G. Forget, B. Cael, M. J. Follows, Moving ecological and biogeochemical transitions across the North Pacific. *Limnol. Oceanogr.* **66**, 2442–2454 (2021).
35. F. Chai, M. Jiang, R. T. Barber, R. C. Dugdale, Y. Chao, Interdecadal variation of the transition zone chlorophyll front: A physical-biological model simulation between 1960 and 1990. *J. Oceanogr.* **59**, 461–475 (2003).
36. M. J. Church, K. M. Björkman, D. M. Karl, M. A. Saito, J. P. Zehr, Regional distributions of nitrogen-fixing bacteria in the Pacific Ocean. *Limnol. Oceanogr.* **53**, 63–77 (2008).
37. J. J. Polovina, E. A. Howell, D. R. Kobayashi, M. P. Seki, The transition zone chlorophyll front updated: Advances from a decade of research. *Prog. Oceanogr.* **150**, 79–85 (2017).
38. J. P. Grover, Resource competition in a variable environment—Phytoplankton growing according to the variable-internal-stores model. *Am. Nat.* **138**, 811–835 (1991).
39. R. A. Armstrong, Grazing limitation and nutrient limitation in marine ecosystems: Steady state solutions of an ecosystem model with multiple food chains. *Limnol. Oceanogr.* **39**, 597–608 (1994).
40. B. A. Biddanda, L. R. Pomeroy, Microbial aggregation and degradation of phytoplankton-derived detritus in seawater. I. Microbial succession. *Mar. Ecol. Prog. Ser.* **42**, 79–88 (1988).
41. M. Goutx *et al.*, Composition and degradation of marine particles with different settling velocities in the northwestern Mediterranean Sea. *Limnol. Oceanogr.* **52**, 1645–1664 (2007).
42. R. W. Sterner, D. O. Hessen, Algal nutrient limitation and the nutrition of aquatic herbivores. *Annu. Rev. Ecol. Syst.* **25**, 1–29 (1994).
43. D. M. Karl, A sea of change: Biogeochemical variability in the North Pacific Subtropical Gyre. *Ecosystems* **2**, 181–214 (1999).
44. N. Kawasaki, R. Sohrin, H. Ogawa, T. Nagata, R. Benner, Bacterial carbon content and the living and detrital bacterial contributions to suspended particulate organic carbon in the North Pacific Ocean. *Aquat. Microb. Ecol.* **62**, 165–176 (2011).
45. D. M. Karl *et al.*, Temporal dynamics of total microbial biomass and particulate detritus at Station ALOHA. *Prog. Oceanogr.* **205**, 102803 (2022).
46. I. A. Hatton *et al.*, The predator-prey power law: Biomass scaling across terrestrial and aquatic biomes. *Science* **349**, aac6284 (2015).
47. M. W. Lomas *et al.*, Varying influence of phytoplankton biodiversity and stoichiometric plasticity on bulk particulate stoichiometry across ocean basins. *Commun. Earth Environ.* **2**, 1–10 (2021).
48. G. Yvon-Durocher, M. Dossena, M. Trimmer, G. Woodward, A. P. Allen, Temperature and the biogeography of algal stoichiometry. *Global Ecol. Biogeogr.* **24**, 562–570 (2015).
49. Z. Finkel, M. Follows, A. Irwin, Size-scaling of macromolecules and chemical energy content in the eukaryotic microalgae. *J. Plankton Res.* **38**, 1151–1162 (2016).
50. B. S. Lambert *et al.*, The dynamic trophic architecture of open-ocean protist communities revealed through machine-guided metatranscriptomics. *Proc. Natl. Acad. Sci. U.S.A.* **119**, e2100916119 (2022).
51. T. Zaviel *et al.*, Quantitative insights into the cyanobacterial cell economy. *eLife* **8**, e42508 (2019).
52. T. Tanioka, K. Matsumoto, A meta-analysis on environmental drivers of marine phytoplankton C:N:P. *Biogeosciences* **17**, 2939–2954 (2020).
53. K. Inomura *et al.*, A mechanistic model of macromolecular allocation, elemental stoichiometry, and growth rate in phytoplankton. *Front. Microbiol.* **11**, 86 (2020).
54. R. Miller *et al.*, Changes in transcript abundance in *Chlamydomonas reinhardtii* following nitrogen-dependent predict diversion of metabolism. *Plant Physiol.* **110**, 165159 (2010).
55. J. D. Liefer *et al.*, The macromolecular basis of phytoplankton C:N:P under nitrogen starvation. *Front. Microbiol.* **10**, 763 (2019).
56. P. Pinedo-González *et al.*, Anthropogenic Asian aerosols provide Fe to the North Pacific Ocean. *Proc. Natl. Acad. Sci. U.S.A.* **117**, 27862–27868 (2020).
57. J. H. Paul, W. H. Jeffrey, M. F. DeFlaun, Dynamics of extracellular DNA in the marine environment. *Appl. Environ. Microbiol.* **53**, 170–179 (1987).
58. C. C. Hannides *et al.*, Export stoichiometry and migrant-mediated flux of phosphorus in the North Pacific Subtropical Gyre. *Deep-Sea Res. I, Oceanogr. Res. Pap.* **56**, 73–88 (2009).
59. E. Saiz, K. Griffell, S. Isari, A. Calbet, Ecophysiological response of marine copepods to dietary elemental imbalances. *Mar. Environ. Res.* **186**, 105940 (2023).
60. C. L. Meunier, J. Haafke, B. Oppermann, M. Boersma, A. M. Malzahn, Dynamic stoichiometric response to food quality fluctuations in the heterotrophic dinoflagellate *Oxyrrhis marina*. *Mar. Biol.* **159**, 2241–2248 (2012).
61. A. Marki, M. Pahlow, Microzooplankton stoichiometric plasticity inferred from modeling mesocosm experiments in the Peruvian upwelling region. *Front. Mar. Sci.* **3**, 258 (2016).
62. R. Huang, B. Wan, M. Hultz, J. M. Diaz, Y. Tang, Phosphatase-mediated hydrolysis of linear polyphosphates. *Environ. Sci. Technol.* **52**, 1183–1190 (2018).
63. T. Rees, J. A. Raven, The maximum growth rate hypothesis is correct for eukaryotic photosynthetic organisms, but not cyanobacteria. *New Phytol.* **230**, 601–611 (2021).
64. G. Y. Rhee, A continuous culture study of phosphate uptake, growth rate and polyphosphate in *Scenedesmus* sp. *J. Phycol.* **9**, 495–506 (1973).
65. C. Mougnot *et al.*, Resource allocation by the marine cyanobacterium *Synechococcus* WH8102 in response to different nutrient supply ratios. *Limnol. Oceanogr.* **60**, 1634–1641 (2015).
66. N. S. Garcia, J. A. Bonachela, A. C. Martiny, Interactions between growth-dependent changes in cell size, nutrient supply and cellular elemental stoichiometry of marine *Synechococcus*. *ISME J.* **10**, 2715–2724 (2016).
67. J. D. H. Strickland, T. R. Parsons, *A Practical Handbook of Seawater Analysis* (Fisheries Research Board of Canada, Ottawa, ON, Canada, 1972), 10.25607/OBP-1791.
68. J. Murphy, J. P. Riley, A modified single solution method for the determination of phosphate in natural waters. *Anal. Chim. Acta* **27**, 31–36 (1962).
69. R. K. Foreman, K. M. Björkman, C. A. Carlson, K. Opalk, D. M. Karl, Improved ultraviolet photo-oxidation system yields estimates for deep-sea dissolved organic nitrogen and phosphorus. *Limnol. Oceanogr. Methods* **17**, 277–291 (2019).
70. R. K. Foreman, M. Segura-Noguera, D. M. Karl, Validation of Ti(III) as a reducing agent in the chemiluminescent determination of nitrate and nitrite in seawater. *Mar. Chem.* **186**, 83–89 (2016).
71. R. R. Holser, M. A. Goni, B. Hales, Design and application of a semi-automated filtration system to study the distribution of particulate organic carbon in the water column of a coastal upwelling system. *Mar. Chem.* **123**, 67–77 (2011).
72. L. Solorzano, J. H. Sharp, Determination of total dissolved phosphorus and particulate phosphorus in natural waters. *Limnol. Oceanogr.* **25**, 754–758 (1980).
73. R. C. Team, *A Language and Environment for Statistical Computing* (R Foundation for Statistical Computing, Vienna, Austria, 2022).
74. F. P. Chavez *et al.*, On the chlorophyll a retention properties of glass-fiber GF/F filters. *Limnol. Oceanogr.* **40**, 428–433 (1995).
75. J. M. Gasol, X. A. Moran, Effects of filtration on bacterial activity and picoplankton community structure as assessed by flow cytometry. *Aquat. Microb. Ecol.* **16**, 251–264 (1999).
76. D. L. Kirchman, R. G. Keil, P. A. Wheeler, The effect of amino acids on ammonium utilization and regeneration by heterotrophic bacteria in the subarctic Pacific. *Deep-Sea Res. A* **36**, 1763–1776 (1989).
77. C. M. Brown, J. D. MacKinnon, A. M. Cockshutt, T. A. Villareal, D. A. Campbell, Flux capacities and acclimation costs in *Trichodesmium* from the Gulf of Mexico. *Mar. Biol.* **154**, 413–422 (2008).
78. S. Bru, J. Jiménez, D. Canadell, J. Ariño, J. Clotet, Improvement of biochemical methods of polyP quantification. *Microb. Cell* **4**, 6 (2017).
79. P. Chen, T. Y. Toribara, H. Warner, Microdetermination of phosphorus. *Anal. Chem.* **28**, 1756–1758 (1956).
80. W. T. Shoaf, B. W. Lium, Improved extraction of chl a and b from algae using dimethyl sulfoxide. *Limnol. Oceanogr.* **21**, 926–928 (1976).
81. T. Masuko *et al.*, Carbohydrate analysis by a phenol-sulfuric acid method in microplate format. *Anal. Biochem.* **339**, 69–72 (2005).
82. J. E. Swallow, F. Ribalet, E. V. Armbrust, SeaFlow: A novel underway flow-cytometer for continuous observations of phytoplankton in the ocean. *Limnol. Oceanogr. Methods* **9**, 466–477 (2011).
83. F. Ribalet *et al.*, SeaFlow data v1, high-resolution abundance, size and biomass of small phytoplankton in the North Pacific. *Sci. Data* **6**, 1–8 (2019).
84. E. A. Moberg, H. M. Sosik, Distance maps to estimate cell volume from two-dimensional plankton images. *Limnol. Oceanogr. Methods* **10**, 278–288 (2012).
85. S. Menden-Deuer, E. J. Lessard, Carbon to volume relationships for dinoflagellates, diatoms, and other protist plankton. *Limnol. Oceanogr. Methods* **45**, 569–579 (2000).
86. A. G. Taylor, M. R. Landry, K. E. Selph, E. J. Yang, Biomass, size structure and depth distributions of the microbial community in the eastern equatorial Pacific. *Deep-Sea Res. 2 Top. Stud. Oceanogr.* **58**, 342–357 (2011).
87. E. Litchman, C. A. Klausmeier, O. M. Schofield, P. G. Falkowski, The role of functional traits and trade-offs in structuring phytoplankton communities: Scaling from cellular to ecosystem level. *Ecol. Lett.* **10**, 1170–1181 (2007).
88. A. E. White, Gradients 2-MGL1704-PPPCPN-UW_2020-03-11_v1.0. Zenodo. <https://doi.org/10.5281/zenodo.4470109>. Deposited 11 March 2020.
89. J. D. Liefer, 2017 Gradients 2 - MGL 1704 Particulate Macromolecules. Zenodo. <https://doi.org/10.5281/zenodo.11582731>. Deposited 17 April 2024.
90. F. Ribalet, *et al.*, SeaFlow Data v1: High-resolution abundance, size and biomass of small phytoplankton in the North Pacific. Zenodo. <https://doi.org/10.5281/zenodo.7102019>. Deposited 21 September 2022.
91. A. E. White, Gradients2-MGL1704-IFCB-ESD_2020-04-01_v1.0. Zenodo. <https://doi.org/10.5281/zenodo.4267135>. Deposited 1 April 2020.
92. K. Cain, F. Ribalet, E. V. Armbrust, Discrete flow cytometry from the Gradients 2017 cruise using a BD Influx Cell Sorter. Zenodo. <https://doi.org/10.5281/zenodo.4085873>. Deposited 13 October 2020.